



Determination of Optimal Indicators Based on Statistical Analysis for the State of Health Estimation of a Lithium-Ion Battery

Gaoya Shi^{1,2}, Siqi Chen^{1,2}, Hao Yuan^{1,2}, Heze You^{1,2}, Xueyuan Wang^{2,3*}, Haifeng Dai^{1,2*} and Xuezhe Wei^{1,2}

¹School of Automotive Studies, Tongji University, Shanghai, China, ²Clean Energy Automotive Engineering Center, Tongji University, Shanghai, China, ³Department of Control Science and Engineering, Tongji University, Shanghai, China

OPEN ACCESS

Edited by:

Caiping Zhang,
Beijing Jiaotong University, China

Reviewed by:

Jinpeng Tian,
Beijing Institute of Technology, China
Kailong Liu,
University of Warwick,
United Kingdom

*Correspondence:

Xueyuan Wang
7wangxueyuan@tongji.edu.cn
Haifeng Dai
tongjidai@tongji.edu.cn

Specialty section:

This article was submitted to
Electrochemical Energy Conversion
and Storage,
a section of the journal
Frontiers in Energy Research

Received: 02 April 2021

Accepted: 17 May 2021

Published: 16 June 2021

Citation:

Shi G, Chen S, Yuan H, You H, Wang X, Dai H and Wei X (2021) Determination of Optimal Indicators Based on Statistical Analysis for the State of Health Estimation of a Lithium-Ion Battery. *Front. Energy Res.* 9:690266. doi: 10.3389/fenrg.2021.690266

Online state of health (SOH) estimation is essential for lithium-ion batteries in a battery management system. As the conventional SOH indicator, the capacity is challenging to be estimated online. Apart from the capacity, various indicators related to the internal resistance are proposed as indicators for the SOH estimation. However, research gaps still exist in terms of optimal resistance-related indicators, online acquisition of indicators, temperature disturbance elimination, and state of charge (SOC) disturbance elimination. In this study, the equivalent circuit model parameters are identified based on recursive least square method in dynamic working conditions in the life span. Statistical analysis methods including multiple stepwise regression analysis and path analysis are introduced to characterize the sensitivity of the parameters to SOH estimation. Based on the above approach, the coupling relationship between the parameters is comprehensively analyzed. Results indicate that the ohmic resistance R_0 and the diffusion capacitance C_d are the most suitable parameters for the SOH indication. Furthermore, R_0 and C_d are proved to be exponentially correlated to the ambient temperature, while SOC demonstrates a quadratic trend on them. To eliminate the disturbance caused by the ambient temperature and SOC, a compensating method is further proposed. Finally, a mapping relationship between SOH and the indicators under normal operations is established. SOH can be estimated with the maximum error of 2.301%, which proves the reliability and feasibility of the proposed indicators and estimation method.

Keywords: lithium-ion battery, state of health, indicator, equivalent circuit model, statistical analysis

INTRODUCTION

Lithium-ion batteries are widely used as the primary energy storage for electric vehicles (EVs), owing to high energy density and low self-discharge rate (Chen et al., 2019; Liu et al., 2019). A reliable battery management system (BMS) is significant in real applications. Among the BMS functions, state of health (SOH) estimation is quite essential for timely maintenance and retirement. And online acquisition of indicators is the premise of the SOH estimation function.

Currently, many studies are conducted for the online SOH estimation of lithium-ion batteries, which involve battery aging mechanism confirmation (Broussely et al., 2005; Agubra and Fergus, 2013), battery life modeling (Ramadass et al., 2004; Gu et al., 2014a), accelerated life testing (Thomas

et al., 2008; Gu et al., 2014b), and the conversion between real applications and lab applications (Takei et al., 2011; Hua et al., 2015; Sun and Xiong, 2015). In these research studies, the SOH indicator is the first and the most important thing.

The capacity and internal resistance of the battery are widely used SOH indicators (Jiang et al., 2019). Many data-driven SOH estimation methods such as support-vector machine (Deng et al., 2016), relevance vector machine (Zheng and Fang, 2015), Gaussian process regression (Liu et al., 2020a; Liu et al., 2020b), and extreme learning machine (Pan et al., 2018) are proposed to estimate SOH based on the capacity. Sliding mode observer (Kim, 2010), genetic algorithm (Chen et al., 2013), total least squares (Chen et al., 2013), Kalman filter (Berecibar et al., 2016), particle filter (Tang et al., 2019), and other improved state estimation methods are also used to quantify SOH with capacity and internal resistance as indicators. Apart from capacity and resistance, other indicators are also proposed in the previous studies. For instance, Bloom (Bloom et al., 2005) used the expression dV/dQ to determine the life state. A similar indicator is also widely suggested (Li et al., 2011; Wang et al., 2011; Han et al., 2014). Moreover, falloff of the battery terminal voltage (Zhou et al., 2016), curves of the terminal voltage during charging (Liu and Chen, 2019; Park et al., 2020), and time spent on a charging/discharging process (Yun and Qin, 2020) are also investigated as the SOH indicators.

Battery capacity is a relatively intuitive SOH indicator. However, the online estimation of the capacity is challenging due to the complexity of the estimation algorithms and the limited variety of inputs available from a cell under operation (Basia et al., 2021; Li et al., 2021). Hence, the SOH estimation methods based on capacity may be limited in EVs. To address this issue, the internal resistance can be utilized as an SOH indicator. At present, many studies have used internal resistance to characterize the SOH. Chen et al. (2013) concluded that the diffusion capacitance could be symbolized to characterize the battery life. Remmlinger et al. (2011) used a sum of the ohmic resistance and the gain of the first-order low-pass transfer-function element representing the polarization effect as the indicator of the battery performance. Wang et al. (2015) and Zenati et al. (2012) employed the ohmic resistance to evaluate the battery life. Furthermore, the charge transfer resistance is also used to characterize the SOH (Wang et al., 2019). Since many kinds of indicators related to the internal resistance are proposed, applicability and sensitivity to the SOH estimation need to be further analyzed for a specific application.

To obtain internal resistance, Zenati et al. (2012) adopted a fuzzy logic system to compute coefficients applied to the ohmic resistance measurements. This method possesses a higher accuracy but requires a higher amount of computation. Chen et al. (2013) used the genetic algorithm to identify the diffusion capacitance. The algorithm is difficult to be implemented online due to high computational complexity. Wang et al. (2019) selected the charge transfer resistance as an SOH indicator and obtained the resistance by fitting the impedance spectroscopy. However, the measurement of the impedance spectra requires supplementary devices (Basia et al., 2021). For online SOH estimation, the indicators should be obtained online.

Besides, there are many uncertainties in actual vehicle operating conditions. For the battery, the state including temperature and state of charge (SOC) will always change; it has a significant impact on the internal resistance (Wang et al., 2019; Wang et al., 2021). Remmlinger et al. (2011), Wang et al. (2015), and other researchers ignored the influence of SOC in their work. Galeotti et al. (2015) studied the variation of internal resistance with SOC and formed a map to consider the effect during the SOH estimation with the internal resistance. However, the influence of temperature on internal resistance was still ignored. In reference (Stroe et al., 2014), the impact of temperature was also not considered. To accurately describe the battery SOH, these factors should be considered.

To fulfill the research gaps, 1) the equivalent circuit model (ECM) parameters are identified based on the recursive least square method (RLSM), facilitating the online implementation; 2) a novel SOH indicator is determined after the applicability and sensitivity analysis on the identified parameters; and 3) a compensating method is proposed to eliminate the disturbance of temperature and SOC to the indicator. Finally, a mapping relationship between the battery SOH and the indicators is established and verified.

EXPERIMENTAL SETUP

Cycle Aging Test

As listed in **Supplementary Table S1**, Cells 1–3 (LFP (8Ah)) are utilized to analyze and determine SOH indicators, and Cells 4–5 (LFP (40Ah) and NCA (2.9Ah)) are used for verification. Besides, Cell 4 is also used to develop the temperature and SOC compensation methods. The cycle aging tests are performed in a climate chamber at 30°C (Cell 2 and Cell 4), 35°C (Cell 1), and 40°C (Cell 3 and Cell 5) for different battery cells. The aging cycle is made up of a CC-CV charge process and a 2C-rate CC discharge process. In the CC-CV charge process, the battery cells are charged at a constant current of 1C-rate until the cutoff voltage is reached, and a constant voltage charge maintains the cutoff voltage until the current decayed to 1/10C-rate. The detailed settings about the charge and discharge processes are available in the Supplementary Material (**Supplementary Table S2**).

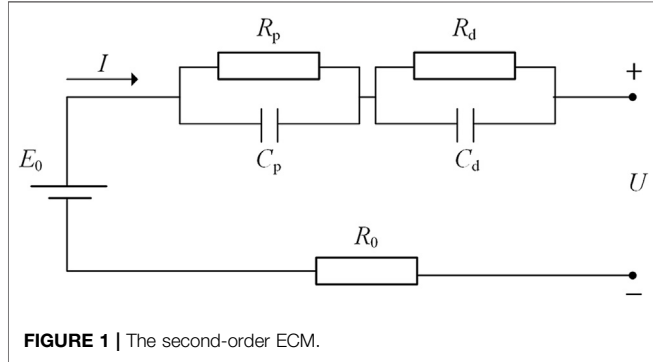
Reference Performance Test

The test matrix for the reference performance test (RPT) is shown in **Table 1**. To identify the ECM parameters, the New European Driving Cycle (NEDC) and the Urban Dynamometer Driving Schedule (UDDS) are used in the RPT. These two operational conditions can excite the battery dynamic characteristic fully, facilitating parameter identification. The battery SOC is set to 60 and 70% for the parameter identification due to the following reasons:

- (1) There exists a large current in the NEDC and UDDS conditions, which may cause transient overpotential phenomena. To avoid the testing failure caused by this issue, a middle SOC range is chosen.
- (2) The open-circuit voltage (OCV) is relatively stable in this SOC range, reducing the error of parameter identification.

TABLE 1 | Test matrix of RPT.

| Test items | Test protocol |
|-----------------------------------|---|
| Capacity calibration | Full charge and full discharge |
| SOC-OCV | Full charge, then discharge to specified SOC (5% SOC interval), and then rest 4 h |
| Internal parameter identification | Internal parameters identified with NEDC and UDDS profiles at 60 and 70% SOC |



Tests for Studying Disturbance of Temperature and State of Charge

According to the operational temperature range of the battery cell in a real application, 5, 15, 25, and 35°C are set in the test to study the evolution of parameters at different temperatures. As for the disturbance of SOC, different SOC (20–80% SOC with 10% SOC interval) are taken into consideration. RPT, as described above, is conducted on Cell 4 at different life stages under these settings.

METHODOLOGY

Parameter Identification Based on an Equivalent Circuit Model

ECM is widely used in the issues of parameter identification since it achieves a trade-off between accuracy and computational efficiency (Schmidt and Skarstad, 1997; Gomez et al., 2011). In the study, parameters identified from the ECM are utilized to construct the mapping relationship between internal parameters and capacity during the aging process. As shown in **Figure 1**, the second-order ECM is adopted to describe the battery dynamics. The specific definitions and explanations of the seven parameters (R_0 , R_p , C_p , R_d , C_d , E_0 , and U) can refer to our previous work (Dai et al., 2016). The difference equation of the battery model is governed by **Eq. 1** (Gomez et al., 2011; Chang et al., 2014).

$$E_{t,k} = (a + b)E_{t,k-1} - abE_{t,k-2} - R_0I_k + [(a + b)R_0 + (a - 1)R_p + (b - 1)R_d]I_{k-1} - [abR_0 + b(a - 1)R_p + a(b - 1)R_d]I_{k-2} = \theta_1E_{t,k-1} + \theta_2E_{t,k-2} + \theta_3I_k + \theta_4I_{k-1} + \theta_5I_{k-2}. \tag{1}$$

where $E_{t,k}$ is the difference between the terminal voltage U and the OCV at time k and I_k is the current at time k . The definitions of a , b , θ_1 , θ_2 , θ_3 , θ_4 , and θ_5 are as follows:

$$a = e^{-\frac{t_s}{R_p C_p}}, \tag{2}$$

$$b = e^{-\frac{t_s}{R_d C_d}}, \tag{3}$$

$$\theta_1 = a + b, \tag{4}$$

$$\theta_2 = -ab, \tag{5}$$

$$\theta_3 = -R_0, \tag{6}$$

$$\theta_4 = [(a + b)R_0 + (a - 1)R_p + (b - 1)R_d], \tag{7}$$

$$\theta_5 = -[abR_0 + b(a - 1)R_p + a(b - 1)R_d]. \tag{8}$$

In the study, the RLSM is used to identify the values of model parameters, that is, θ_1 , θ_2 , θ_3 , θ_4 , and θ_5 (Dai et al., 2016). Once θ_1 , θ_2 , θ_3 , θ_4 , and θ_5 are known, ECM parameters can be calculated by **Eqs. 9–14**:

$$R_0 = -\theta_3, \tag{9}$$

$$R_p = \frac{a\theta_4 + \theta_5 - a^2R_0}{(a - 1)(a - b)}, \tag{10}$$

$$R_d = \frac{b\theta_4 + \theta_5 - b^2R_0}{(b - 1)(b - a)}, \tag{11}$$

$$C_p = \frac{-t_s}{R_p \ln a}, \tag{12}$$

$$C_d = \frac{-t_s}{R_d \ln b}, \tag{13}$$

$$a, b = \frac{\theta_1 \pm \sqrt{\theta_1^2 - 4\theta_2}}{2}. \tag{14}$$

Statistical Analysis of Equivalent Circuit Model Parameters

To find the most sensitive SOH indicators, typical multivariate analysis methods including multiple stepwise regression analysis (MSRA) and path analysis (PA) are used to analyze the coupling relationship between the ECM parameters during the whole life span.

Principle of Multiple Stepwise Regression Analysis

MSRA introduces the parameters into the characteristic equation one by one and removes the low-priority parameters based on some statistical indexes. The typical statistical indexes for judging whether a statistical variable satisfies the significant requirements include F -statistic, t -statistic, p -statistic, and R -squared. The F -statistic represents the degree of similarity between the

sample and the population. A bigger *F*-statistic value represents the better effectiveness of sample data. The *t*-statistic can be used to evaluate the significance of each variable contained in the final regression equation. A bigger *t*-statistic value means that the variable is more significant. The thresholds of the *t*-statistic value at different significance levels are illustrated in **Supplementary Table S3**. When the significance level is lower than 0.05, the regression equation can be established. The *p*-statistic describes the error probability of the regression equation. A smaller *p*-statistic value means a smaller error. When the *p*-statistic value is higher than 0.05, the regression equation cannot be established. *R*-squared value reflects the fitting effect of the model. The closer the *R*-squared value is to 1, the better the fitting effect is.

Primary ECM parameters related to battery life span are initially extracted through MSRA, and then the regression equation between the selected parameters and SOH is established. Furthermore, the *p*-statistic value and *R*-squared value are used to evaluate the established model. The detailed calculation process of MSRA can be found in the study by Nghiep and Al (2001) and Stolzenberg (2004).

Principle of Path Analysis

Each ECM parameter has a particular mapping relationship with battery capacity. For a specific parameter, this mapping relationship is not only related to its direct impact but also affected by the coupling relationship with the other parameters. PA can be utilized to analyze the coupling relationship between characteristic parameters (Stage et al., 2004), which is beneficial to acquire the direct influence of each parameter on the mapping relationship and mine the indirect impact on the other parameters by a correlation coefficient, direct path coefficient, and indirect path coefficient. Furthermore, the direct or indirect influence can be quantified through numerical models (Park et al., 2021).

The method is briefly described as follows. A multiple linear regression equation is established as Eq. 15.

$$y = b_0 + b_1x_1 + b_2x_2 + \dots + b_mx_m, \tag{15}$$

where $\{x_i, i = 1, 2, \dots, m\}$ are the independent variables and *y* is the dependent variable. The following equation can be obtained by averaging the independent variables and the dependent variable.

$$\bar{y} = b_0 + b_1\bar{x}_1 + b_2\bar{x}_2 + \dots + b_m\bar{x}_m. \tag{16}$$

Combining the above two equations, the following equation can be acquired:

$$\begin{aligned} \frac{y - \bar{y}}{\sigma_y} &= b_1 \frac{(x_1 - \bar{x}_1)}{\sigma_y} + \dots + b_m \frac{(x_m - \bar{x}_m)}{\sigma_y} \\ &= b_1 \frac{\sigma_{x_1}}{\sigma_y} \frac{(x_1 - \bar{x}_1)}{\sigma_{x_1}} + \dots + b_m \frac{\sigma_{x_m}}{\sigma_y} \frac{(x_m - \bar{x}_m)}{\sigma_{x_m}}, \end{aligned} \tag{17}$$

where $\{\sigma_{x_i}, i = 1, 2, \dots, m\}$ are the standard deviations of the independent variables and $\left\{ b_i \frac{\sigma_{x_i}}{\sigma_y}, i = 1, 2, \dots, m \right\}$ are the standardized partial regression coefficients (the direct path coefficients), which represent the direct influence of each

independent variable on the dependent variable. Then, a series of complex calculations are conducted (Alwin and Hauser, 1975), and the mathematical model of PA is described as

$$\begin{cases} P_{1Y} + r_{12}P_{2Y} + r_{13}P_{3Y} + \dots + r_{1m}P_{mY} = r_{1Y} \\ r_{21}P_{1Y} + P_{2Y} + r_{23}P_{3Y} + \dots + r_{2m}P_{mY} = r_{2Y} \\ \dots \\ r_{m1}P_{1Y} + r_{m2}P_{2Y} + r_{m3}P_{3Y} + \dots + P_{mY} = r_{mY} \end{cases}, \tag{18}$$

where r_{ij} is the correlation coefficient between variable x_i and x_j and P_{iY} is the direct path coefficient. $r_{ij}P_{jY}$ is the indirect path coefficient, which means that x_i affects y through x_j ($x_i \rightarrow x_j \rightarrow Y$). It can be observed that the correlation coefficient r_{iY} is decomposed into the direct path coefficient P_{iY} and the sum of the indirect path coefficients $\sum r_{ij}P_{jY}$.

Definition of State of Health Considering Disturbance of Temperature and State of Charge

The ECM parameters generally fluctuate with temperature and SOC even in the same battery aging state, which affects the reliability of the SOH definition. Hence, additional tests are conducted to reveal the disturbance of temperature and SOC. The SOH definition is modified accordingly. Moreover, the accuracy of the modified SOH definition will be verified by further battery life tests. The approach for SOH indicator determination proposed in this work is depicted in **Figure 2**.

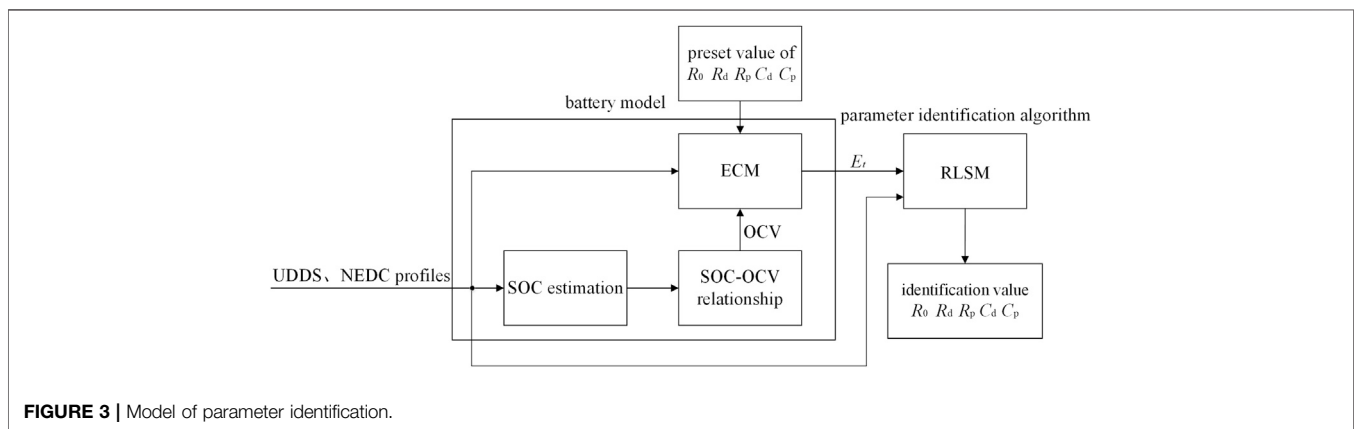
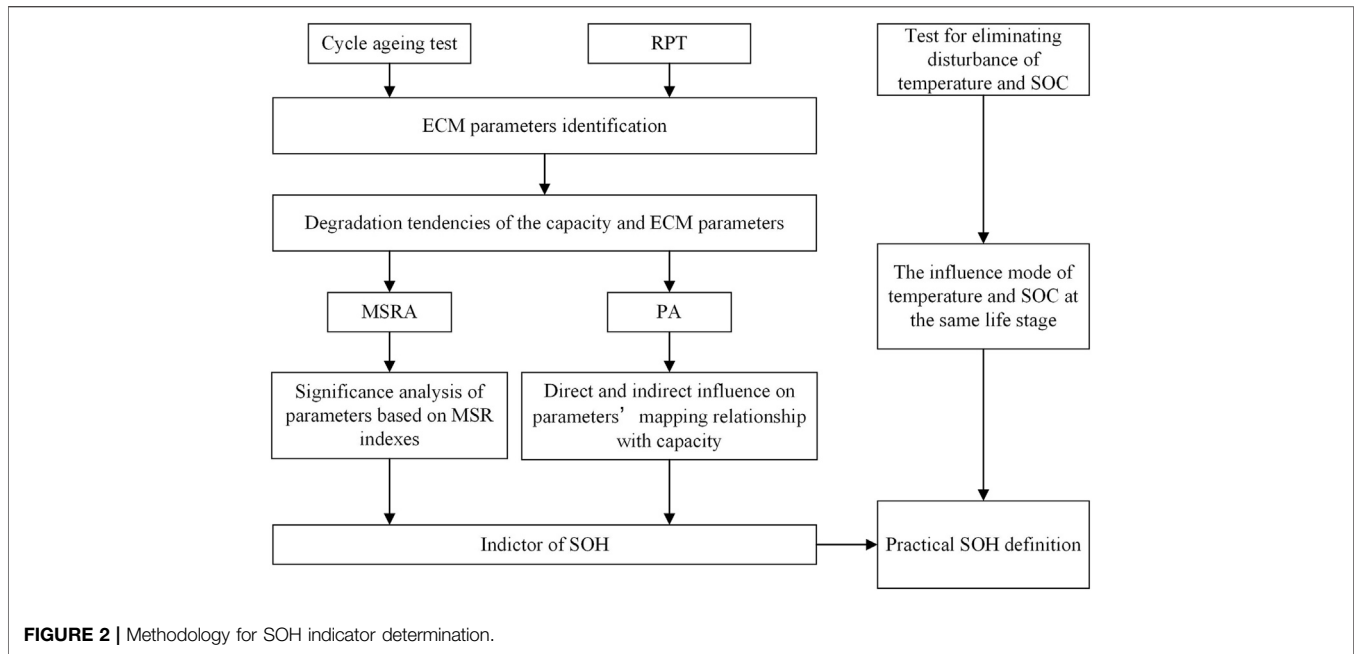
RESULTS AND DISCUSSION

Verification of Parameter Identification Method

The identification model for the ECM parameters is shown in **Figure 3**. The process is carried out in Matlab/Simulink. Coulomb counting is used to estimate SOC during the experiments. The current can be precisely measured by the battery tester, which leads to a tiny error during the Coulomb counting. Therefore, SOC estimation is considered accurate enough during the experiments.

Further, the real-time value of OCV can be calculated based on the predefined SOC–OCV relationship, which originated from RPT in *Experimental Setup*. The terminal voltage *U* minus OCV of the ECM is the modeled voltage response E_t required by the identification algorithm. The ECM parameters are identified based on the RLSM. To verify the accuracy of the identification method, the values of ECM parameters are preset, and the model is then tested with current profiles of UDDS and NEDC.

The validation test is carried out four times. By comparing the identified results with the preset values of ECM parameters, the accuracy of the identification method can be validated. The comparison results in different life stages under UDDS current profile are shown in **Supplementary Figure S1**. The identification values of R_0 , R_d , R_p , and C_d are approximately equal to their preset values. However, there is a relative error of about 3% in



identifying C_p (within the tolerance). A similar conclusion can be drawn in the NEDC condition. R_0 , R_d , R_p , and C_d can be accurately estimated, and for the polarization capacitance C_p , the error is within 4%.

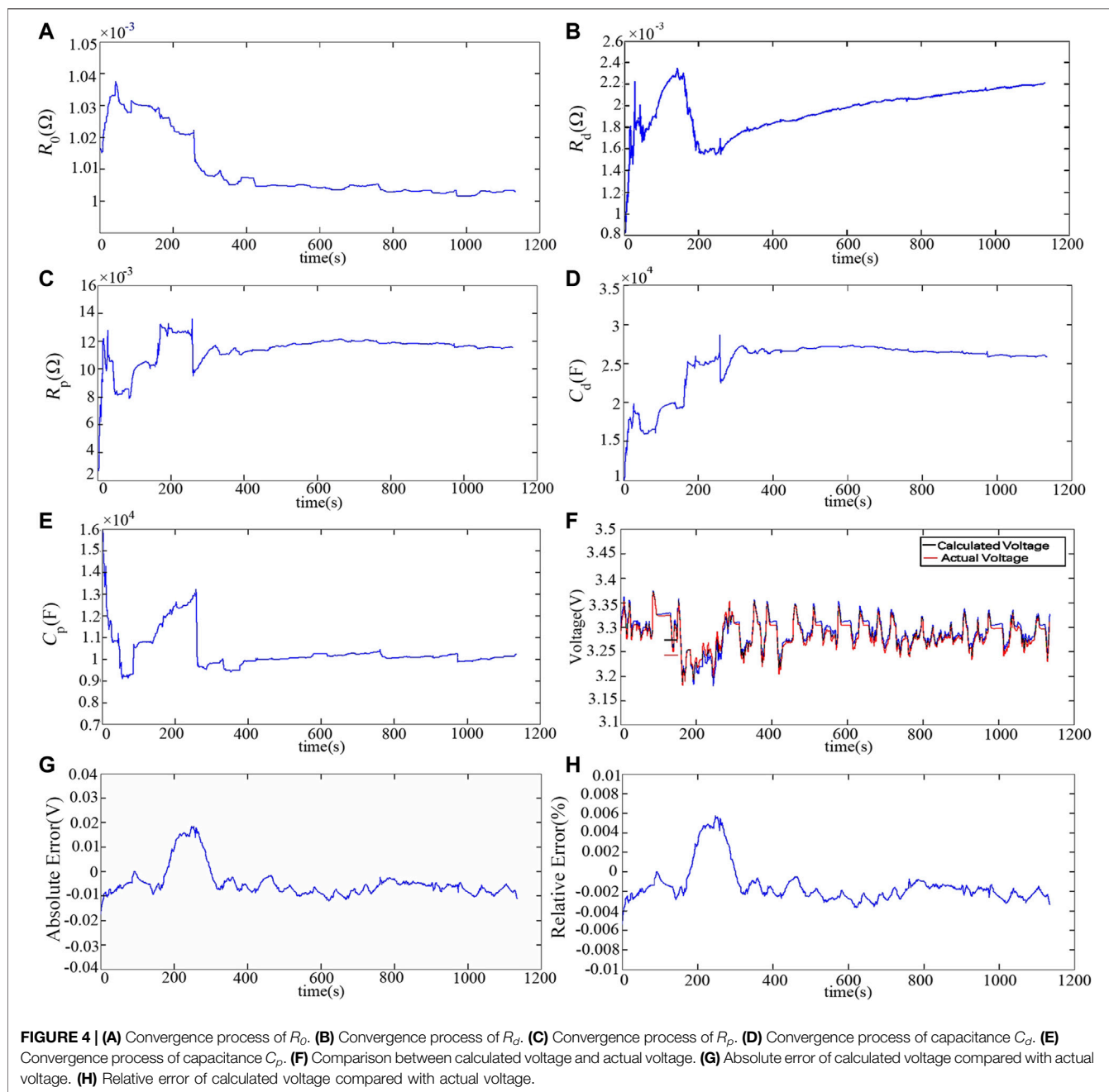
Degradation Tendency of Equivalent Circuit Model Parameters

UDDS and NEDC current profiles are loaded to the battery on the testing bench, and the actual values of response voltage and current can be obtained and put into the identification algorithm. Accordingly, the ECM parameters can be identified. The convergence process of each parameter identification under the UDSS current profile is shown in **Figures 4A–E**. The convergence time of each parameter is similar: about 300 s.

In previous studies of battery model parameter identification, the performance of the identification is generally validated by

comparing the modeled voltage and the actual voltage. The modeled voltage is obtained by the following method. The ECM parameters are set in the above parameter identification model to the identification results obtained by the RLSM with the input (the actual values of response voltage and current). The modeled voltage response E_t can be calculated by the ECM module. As shown in **Figure 4F**, the modeled voltage matches the actual voltage well. The absolute error and the relative error are displayed in **Figures 4G,H**. The maximum absolute error is 0.0184 V, and the maximum relative error is just 0.57%. The result under the NEDS current profile is similar. The maximum absolute error is 0.0299 V, and the relative error is within 0.96%. Therefore, the proposed identification method is reliable and reasonable.

The ECM parameters during the whole lifetime are estimated based on the aforementioned identification method. Accordingly, the degradation tendency of each parameter can be obtained.



Subsequently, the results are statistically analyzed to explore the relationships between the ECM parameters and the battery capacity to extract the optimal SOH indicators. In the study, the normalized values of ECM parameters are adopted for eliminating the errors caused by the difference between different physical units.

For the LFP battery with a nominal capacity of 8Ah (Cell 1–Cell 3), the degradation tendencies of the ECM parameters identified at 70% SOC during the whole lifetime are depicted in **Figure 5**. With the battery aging, R_0 , R_p , and R_d increase, while C_p and C_d decrease, which is similar to the verification batteries (Cell 4 and Cell 5) drawn in

Supplementary Figure S2. Hence, these five parameters can all be used as SOH indicators to characterize the battery life. For batteries at 60% SOC, the same conclusion can be obtained.

Determination of State of Health Indicators Based on Statistical Analysis

As mentioned above, the five ECM parameters can be used to characterize the battery SOH. However, their mapping relationship with the capacity varies. The mapping relationship between some parameters and the capacity is noticeable, while the

TABLE 2 | Indexes of MSR for Cell 1.

| | Parameters | F-value | t-value | p-value | R-square |
|-----|------------|----------|---------|---------|----------|
| 1st | R_0 | 54.1477 | -7.3585 | 0.0002 | 0.8855 |
| | R_p | 52.3015 | -7.2320 | 0.0002 | 0.8820 |
| | C_p | 10.9145 | 3.3037 | 0.0131 | 0.6093 |
| | R_d | 12.2831 | -3.5047 | 0.0099 | 0.6370 |
| | C_d | 35.2653 | 5.9385 | 0.0006 | 0.8344 |
| 2nd | R_p | 24.4751 | -0.5390 | 0.6093 | 0.8908 |
| | C_p | 26.0875 | -0.8122 | 0.4477 | 0.8969 |
| | R_d | 24.7204 | -0.5888 | 0.5775 | 0.8918 |
| | C_d | 408.3480 | 9.3904 | 0.0001 | 0.9927 |
| 3rd | R_p | 242.5520 | -0.5859 | 0.5834 | 0.9932 |
| | C_p | 283.4710 | -1.1129 | 0.3164 | 0.9942 |
| | R_d | 353.1780 | 1.6625 | 0.1573 | 0.9953 |

other parameters cannot reflect the capacity evolution. In this section, MSRA and PA are used to find indicators considerably correlated with the capacity.

Multiple Stepwise Regression Analysis of Equivalent Circuit Model Parameters

Parameters of Cell 1 identified at 70% SOC are taken as an example for MSRA. The normalized values of the parameters at different life stages are available in the Supplementary Material (**Supplementary Figure S3A**). The indexes of MSR for each parameter are listed in **Table 2**. Note that there are three analysis results of MSR indexes in **Table 2**. Here is the first analysis. As mentioned in the *Principle of Multiple Stepwise Regression Analysis*, when the values of F-statistic, t-statistic, and R-square are higher, the p-statistic is smaller, and the parameter will be more significant. Hence, the relationship between the ohmic resistance R_0 and the battery capacity is apparent.

After removing R_0 , MSRA is performed again for the remaining ECM parameters. The second analysis in **Table 2** gives out the indexes for the remaining four parameters, revealing that C_d is another parameter in the regression equation.

In MSRA, when multiple parameters appear in the regression equation due to the coupling relationship between these

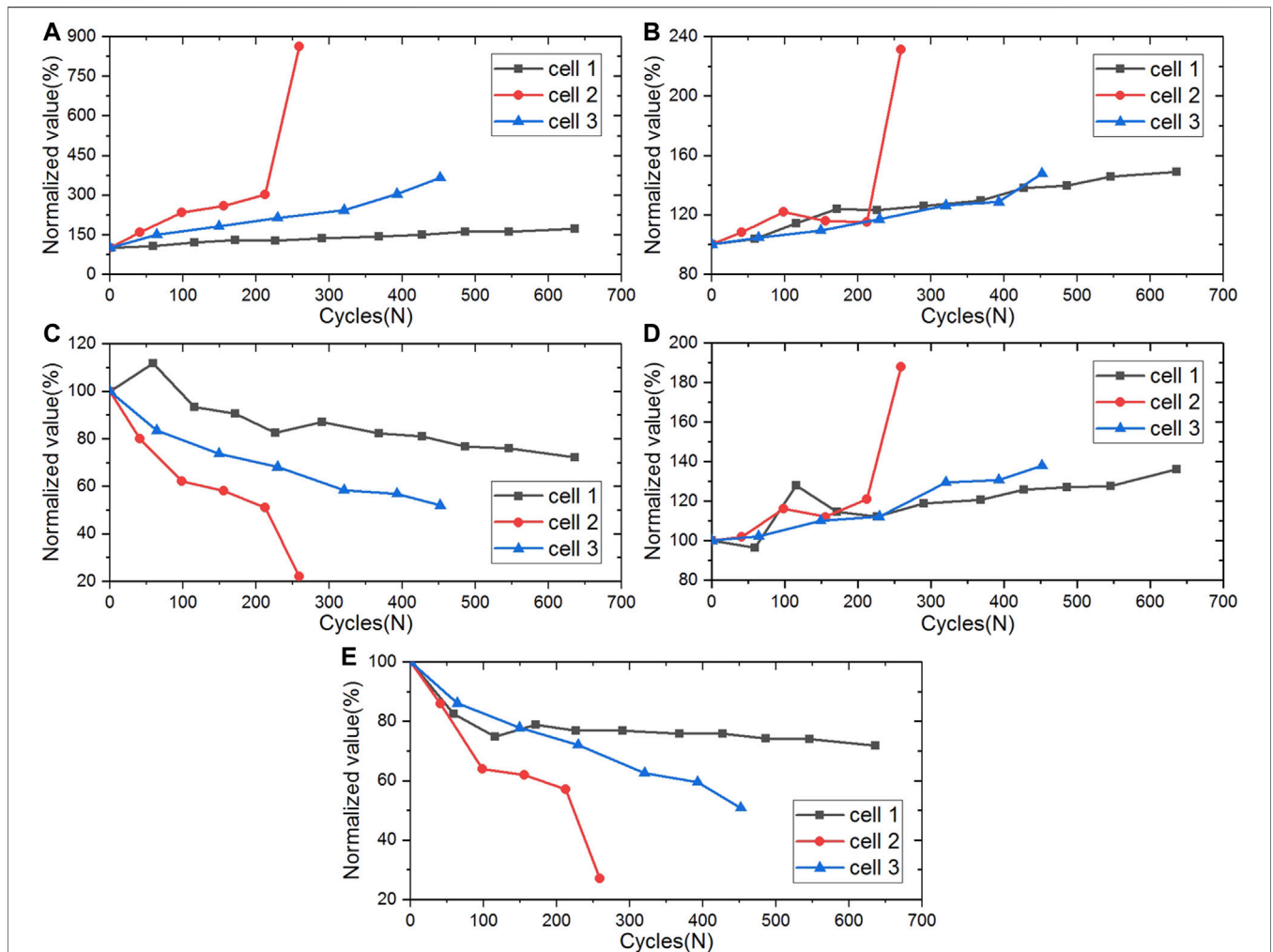


FIGURE 5 | Degradation tendencies of ECM parameters under 70% SOC for Cells 1-3: (A) R_0 , (B) R_p , (C) C_p , (D) R_d , and (E) C_d .

TABLE 3 | Correlation coefficient between parameters of Cell 1 (70% SOC).

| Parameter | R_0 | R_p | C_p | R_d | C_d | Capacity |
|-----------|---------|---------|---------|---------|--------|----------|
| R_0 | 1 | | | | | |
| R_p | 0.9844 | 1 | | | | |
| C_p | -0.8827 | -0.9072 | 1 | | | |
| R_d | 0.7974 | 0.7957 | -0.7929 | 1 | | |
| C_d | -0.7347 | -0.7419 | 0.5810 | -0.7435 | 1 | |
| Capacity | -0.9410 | -0.9391 | 0.7805 | -0.7981 | 0.9134 | 1 |

parameters, it is necessary to analyze the significance of each parameter to determine whether there are parameters that need to be removed from the equation. The t -statistic value of R_0 is -11.4129 and that of C_d is 9.3904 . Furthermore, their p -statistic values are both close to 0. Therefore, R_0 and C_d are both essential parameters. These parameters should be kept in the regression equation.

The MSR indexes of the remaining three parameters are calculated again. The third analysis in **Table 2** shows that the most critical parameter is R_d . However, the t -statistic value is less than 2.365 (sample size is 9), and the p -statistic value is more than 0.05, which cannot meet the lowest requirement for entry into the regression equation described in *Principle of Multiple Stepwise Regression Analysis*. Similarly, the other ECM parameters cannot be introduced into the regression equation. So far, the MSRA is finished. The ohmic resistance R_0 and the capacitance C_d are the most suitable indicators of the battery life for Cell 1 at 70% SOC. The final linear equation characterizing SOH is expressed with

$$SOH = -0.1343R_0 + 0.2641C_d + 0.8685. \quad (19)$$

Moreover, MSRA is also performed on the same battery (Cell 1) calibrated at 60% SOC, and **Supplementary Figure S3B** exhibits the normalized values of ECM parameters. The critical parameters include ohmic resistance R_0 , capacitance C_d , and resistance R_p . And the linear regression equation is established as **Eq. 20**.

$$SOH = -0.0844R_0 - 0.1147R_p + 0.3924C_d + 0.8049. \quad (20)$$

From **Eqs. 19** and **20**, it is found that the SOH indicators are different for the same battery at different SOCs. Therefore, it is not easy to obtain the general SOH indicators only through MSRA. The same conclusion can be obtained in the MSRA of Cell 2. The most critical parameters are R_d and C_d for Cell 2 at 70% SOC. However, only C_d is selected as the indicator for Cell 2 at 60% SOC.

To summarize, SOH can be defined by MSRA, but for the same battery at different SOCs or different batteries at the same SOC, the SOH indicators are not the same. Therefore, pure MSRA cannot obtain stable SOH indicators, and PA is proposed to achieve this objective.

Path Analysis of Equivalent Circuit Model Parameters

(1) Analysis of Cell 1 at 70% SOC

Table 3 shows the correlation coefficients between ECM parameters. The positive coefficient represents a positive correlation, the negative coefficient means negatively

correlated, and the degree of correlation is determined by the absolute value of the coefficient. The correlation coefficient thresholds at different significance levels (P) are illustrated in **Supplementary Table S4**. There is a significant relationship between two variables when $p < 0.05$ and an extremely significant relationship when $p < 0.01$. For Cell 1 at 70% SOC, it can be observed that the correlation coefficient thresholds of the significant level and the extremely significant level are 0.666 and 0.798, respectively. From **Table 3**, although there is no significant correlation between C_p and C_d , the correlation coefficients between all other parameter pairs have reached a high level. There are even quite a few parameter pairs that have an extremely significant relationship. Thus, there is a complicated coupling relationship between the abovementioned parameters.

The direct path coefficients and the indirect path coefficients of ECM parameters can be calculated as introduced in *Principle of path analysis*, and the result is demonstrated in **Table 4**. The bold numbers on the diagonal line in **Table 4** are the direct path coefficients between each ECM parameter and battery capacity. The rightmost column of the table is the correlation coefficients between each parameter and capacity, as mentioned in **Table 3**. The remaining numbers are the indirect path coefficients. Each parameter has four indirect path coefficients since its mapping relationship with capacity can be affected by the four coupling relationships between it and the remaining four parameters. This coupling relationship is considered an indirect influence. The positive and negative of the path coefficient represent the positive and negative influence, and the absolute value of the path coefficient represents the degree of influence. Notably, the correlation coefficient of each parameter is equal to the direct path coefficient plus the sum of all indirect path coefficients.

The analysis for **Table 4** is described as follows:

- The correlation coefficient indicates the significance of each parameter's mapping relationship with capacity. Accordingly, the order of the ECM parameters' relevance is $R_0 > R_p > C_d > R_d > C_p$. However, the order does not mean that R_0 can be used as an SOH indicator, and C_p does not have this potential. As elaborated above, the correlation coefficient is equal to the direct path coefficient plus the sum of all indirect path coefficients. Therefore, it can be concluded that the above mapping relationship includes the direct influence and the indirect influence from the other parameters.
- The correlation coefficient between C_d and the battery capacity reaches a high level (0.9134), and the direct path coefficient between them is the highest (0.4751). The indirect path coefficient of C_d through R_0 is larger, and that through other parameters are relatively small, which indicates that the significant mapping relationship between C_d and capacity is mainly affected by itself and the indirect influences through C_d and R_0 .
- The direct path coefficient and the correlation coefficient between R_0 and capacity are both considerable. Hence, R_0 is an essential factor. C_d plays a principal role in the indirect influence by analyzing the indirect path coefficients of R_0 .

TABLE 4 | Direct path coefficient and indirect path coefficient of Cell 1 (70% SOC).

| | R_0 | R_p | C_p | R_d | C_d | Correlation coefficient with capacity |
|-------|----------------|----------------|----------------|---------------|---------------|---------------------------------------|
| R_0 | -0.4581 | -0.2734 | 0.0942 | 0.0453 | -0.3490 | -0.9410 |
| R_p | -0.4510 | -0.2777 | 0.0968 | 0.0452 | -0.3525 | -0.9391 |
| C_p | 0.4044 | 0.2519 | -0.1067 | -0.0450 | 0.2760 | 0.7805 |
| R_d | -0.3653 | -0.2210 | 0.0846 | 0.0568 | -0.3532 | -0.7981 |
| C_d | 0.3366 | 0.2060 | -0.0620 | -0.0422 | 0.4751 | 0.9134 |

The bold values are the direct path coefficients between each ECM parameter and battery capacity.

TABLE 5 | Direct path coefficient and indirect path coefficient of Cell 1 (60% SOC).

| | R_0 | R_p | C_p | R_d | C_d | Correlation coefficient with capacity |
|-------|----------------|----------------|----------------|---------------|---------------|---------------------------------------|
| R_0 | -0.4654 | -0.2026 | 0.0628 | 0.0159 | -0.3623 | -0.9515 |
| R_p | -0.4087 | -0.2308 | 0.0555 | 0.0099 | -0.3372 | -0.9112 |
| C_p | 0.4095 | 0.1795 | -0.0714 | -0.0174 | 0.2418 | 0.7420 |
| R_d | -0.3178 | -0.0980 | 0.0533 | 0.0234 | -0.2377 | -0.5769 |
| C_d | 0.3922 | 0.1810 | -0.0402 | -0.0129 | 0.4299 | 0.9500 |

The bold values are the direct path coefficients between each ECM parameter and battery capacity.

(d) The correlation coefficient between R_p and capacity is also relatively large, ranking the second among all five ECM parameters. Noted that the indirect influences through R_0 (-0.4510) and C_d (-0.3525) are higher than the direct influence of R_p itself (-0.2777). Conversely, the indirect influences through C_p and R_d have almost no contribution to the mapping relationship of R_p with capacity. It can be concluded that the mapping relationship between R_p and capacity mainly results from the effects of R_0 and C_d , and R_p is not suitable as an SOH indicator.

(e) For C_p and R_d , although the correlation coefficients have reached a significant level, the direct path coefficients between them and the battery capacity are small. The significant correlation coefficient is caused by the indirect influences of R_0 and C_d . Hence, C_p and R_d have no potential as SOH indicators.

Based on the above analysis, the ohmic resistance R_0 and the capacitance C_d are considered to be the optimal SOH indicators for Cell 1 at 70% SOC. The expression of SOH is shown in **Supplementary Table S5**.

(2) Analysis of Cell 1 at 60% SOC

The PA process of Cell 1 at 60% SOC is the same as above. There are also complicated coupling relationships between the ECM parameters. The direct path coefficients and the indirect path coefficients of ECM parameters are documented in **Table 5**. The significance of the five parameters can be sorted as $R_0 > C_d > R_p > C_p > R_d$. There is a considerable mapping relationship between R_0 and the capacity caused by itself and the indirect

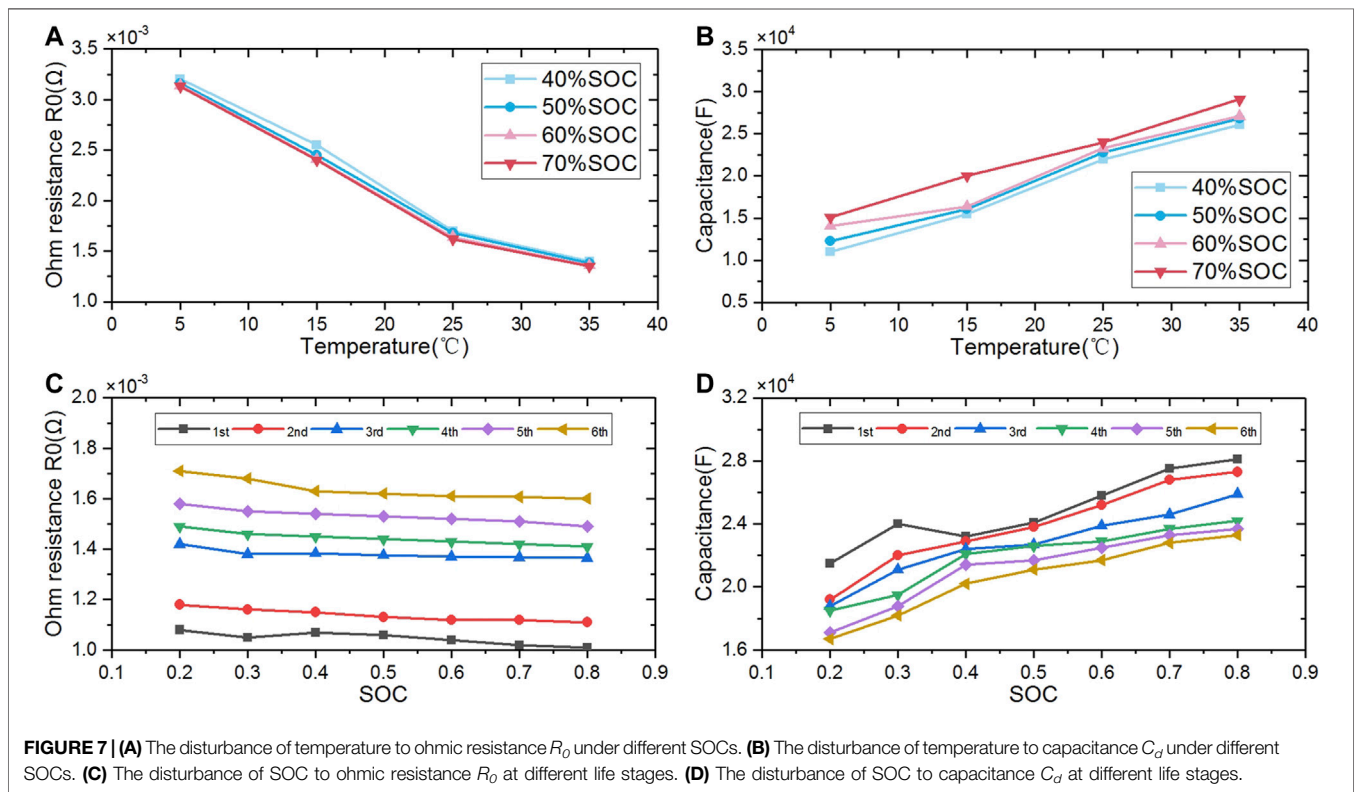
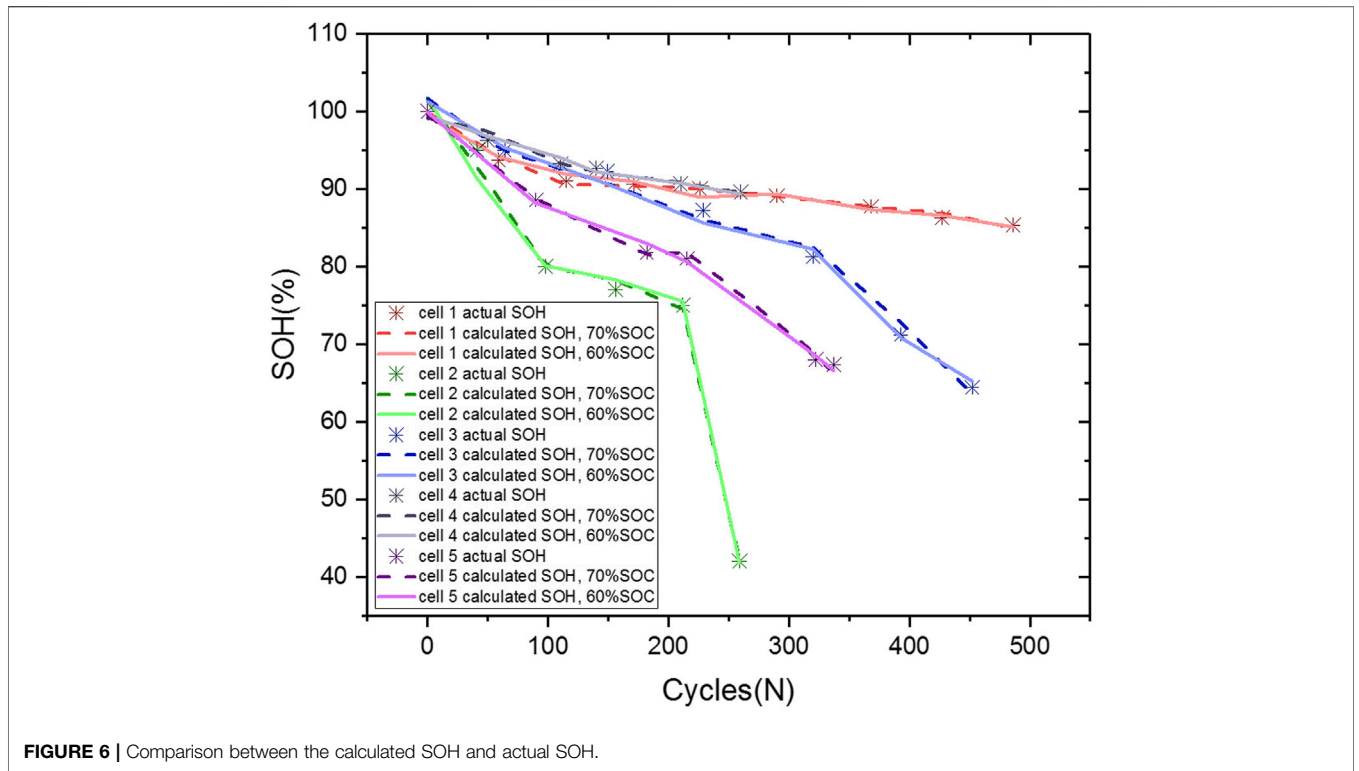
influence through C_d . The direct path coefficient of C_d and its indirect path coefficient through R_0 are also significant. The direct influences of R_p , C_p , and R_d on their mapping relationships with battery capacity are not apparent, but their indirect influences through R_0 and C_d are evident. Hence, the same conclusion can be drawn as the above Cell 1 at 70% SOC. R_0 and C_d are selected as the SOH indicators. Moreover, its SOH expression is also demonstrated in **Supplementary Table S5**.

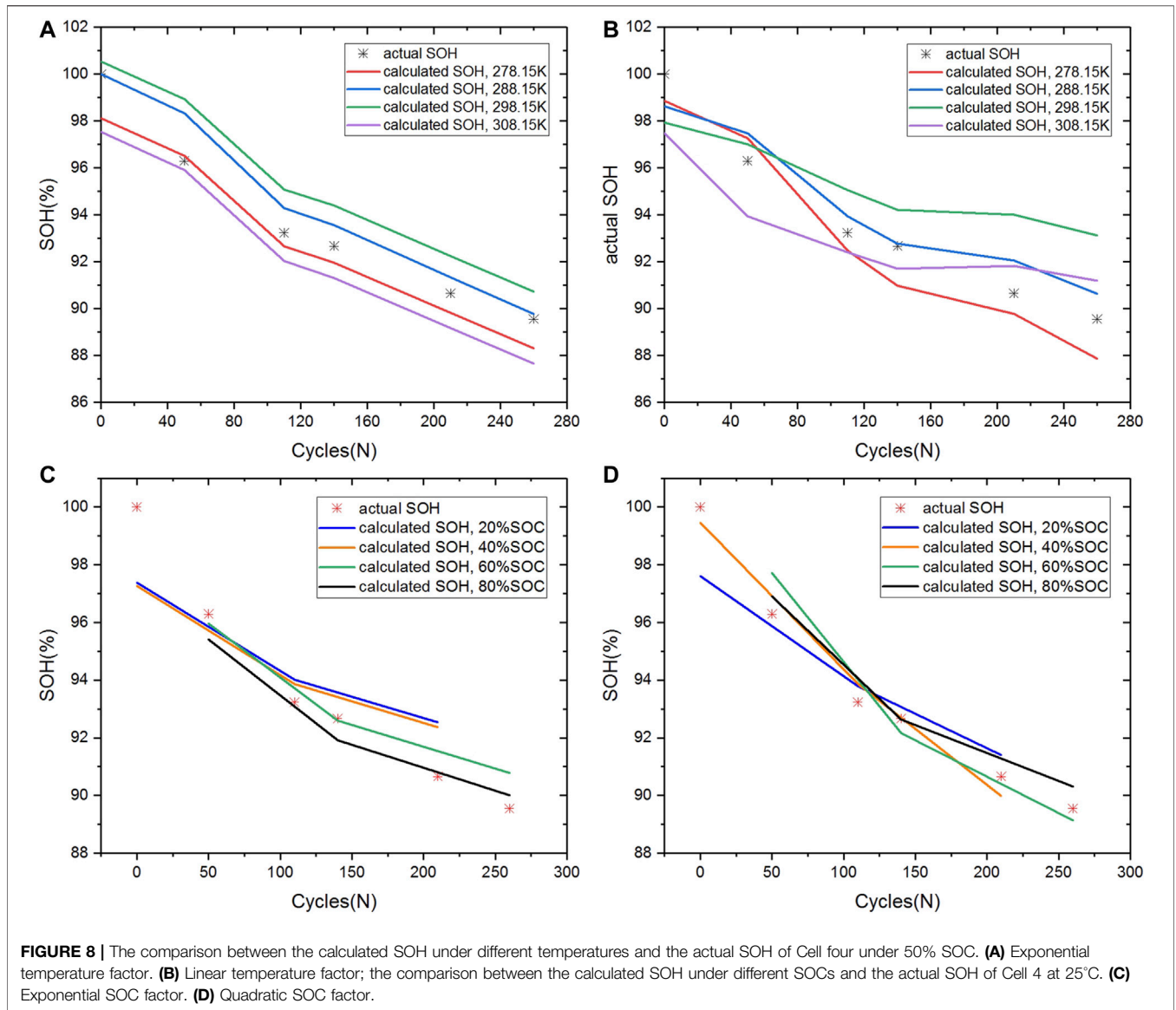
(3) Analysis of Cells 2–5

The accelerated aging test temperature of Cell 2 (30°C) and Cell 3 (40°C) is different from that of Cell 1 (35°C). The same PA is carried out on them. Combining the analysis results of the correlation coefficient, direct path coefficient, and indirect path coefficient, the ohmic resistance R_0 and capacitance C_d can be determined as the primary SOH indicators, which are consistent with the conclusion of Cell 1. The nominal capacity of Cell 4 (40Ah) is varied from that of Cells 1–3 (8Ah), and the type of Cell 5 (NCA) is different from that of Cells 1–3 (LFP). PA is conducted on Cell 4 and Cell 5 at 60% SOC and 70% SOC to investigate whether the above conclusions are universal. Since the analysis process is the same as above, there is no need to repeat it. The same as in Cells 1–3, the final SOH indicators are R_0 and C_d . Their SOH expressions are demonstrated in **Supplementary Table S5**.

Verification of State of Health Definition

According to the above analysis, the SOH expressions of Cells 1–5 at different SOC levels can be obtained, as shown in **Supplementary Table S5**. The comparison of the actual SOH and calculated SOH derived from the above SOH expressions is illustrated in **Figure 6**.





The calculated SOH at different SOC of all the cells reproduces the experimental results with a maximum error of 2.8%. Therefore, as long as the real-time values of R_0 and C_d are identified online, SOH can be accurately estimated.

Modification of State of Health Considering Ambient Temperature and State of Charge

Since the ECM parameters are easily affected by ambient temperature and SOC, the definition of SOH in the previous section needs to be revised.

Disturbance of Temperature to State of Health Indicators

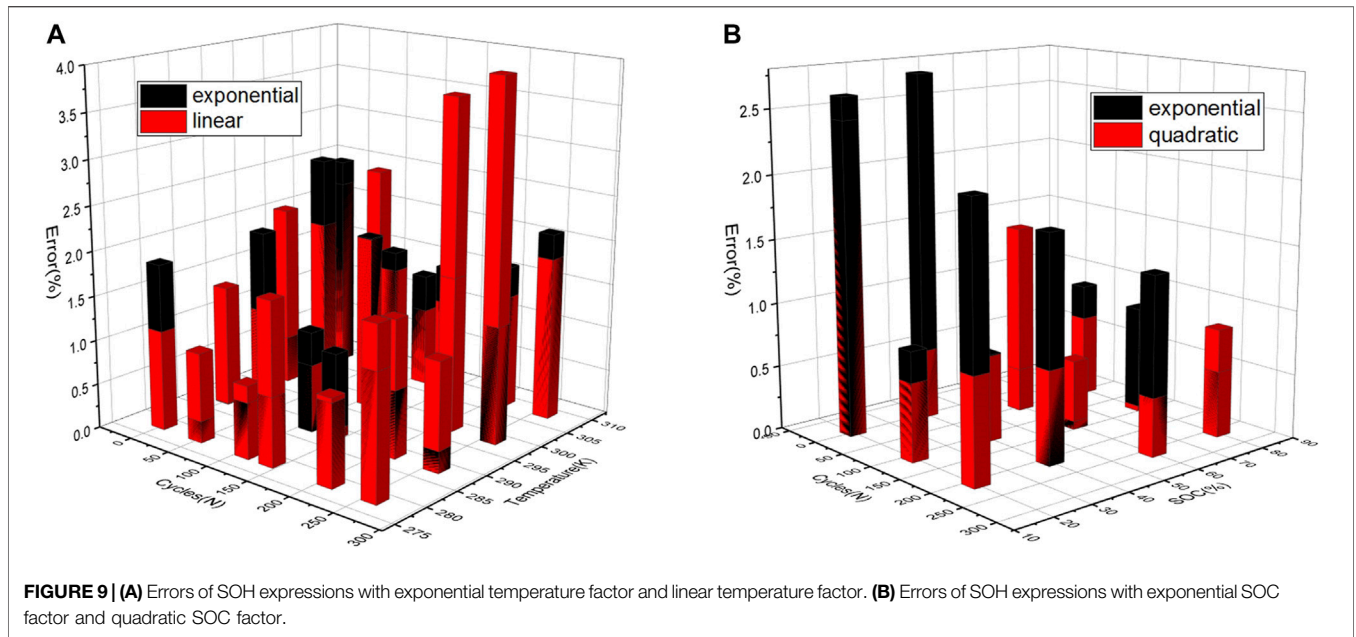
The ECM parameters of Cell 4 are identified at different temperatures to investigate the evolutions of R_0 and C_d . **Figures**

7A and B present the variations of SOH indicators at different temperatures. It is apparent that R_0 decreases and C_d increases as the temperature increases. Furthermore, the variation laws are similar for various SOC. 50% SOC is selected to investigate the modified expression of SOH. The SOH definition based on the method in *Determination of State of Health Indicators Based on Statistical Analysis* is expressed as follows:

$$SOH = -0.1R_0 + 0.4641C_d + 0.6255. \tag{21}$$

According to **Figures 7A and B**, temperature and the two SOH indicators are both considered to be exponentially or linearly correlated. Their expressions are as follows:

$$SOH = -0.1R_0 \times e^{\alpha\left(\frac{1}{T}-\frac{1}{T_{ref}}\right)} + 0.4641C_d \times e^{\beta\left(\frac{1}{T}-\frac{1}{T_{ref}}\right)} + 0.6255 + \varphi', \tag{22}$$



$$SOH = -0.1R_0 \times \gamma \frac{T}{T_{ref}} + 0.4641C_d \times \varepsilon \frac{T}{T_{ref}} + 0.6255 + \theta, \quad (23)$$

where T is the absolute temperature and T_{ref} is the reference temperature set to 25°C (298.15 K). $\alpha, \beta, \varphi, \gamma, \varepsilon,$ and θ are the calibration parameters determined by curve fitting. After fitting, the modified SOH expressions are

$$SOH = -0.1R_0 \times e^{-2433\left(\frac{1}{T} - \frac{1}{T_{ref}}\right)} + 0.4641C_d \times e^{2334\left(\frac{1}{T} - \frac{1}{T_{ref}}\right)} + 0.6413, \quad (24)$$

$$SOH = 1.3055 \frac{R_0 T}{T_{ref}} + 0.4674 \frac{C_d T}{T_{ref}} + 1.3268. \quad (25)$$

The results of performing exponential and linear temperature factors are shown in **Figures 8A,B**, respectively. **Figure 9A** reveals the error in the above two SOH expressions to compare the accuracy of the exponential trend and the linear trend. The maximum error of the exponential trend is 2.74% at 25°C (298.15 K), while the maximum error of the linear trend is 3.99% at 25°C (298.15 K). Moreover, the overall error of the linear trend is more significant than that of the exponential trend. Therefore, it can be concluded that the disturbance of temperature to the SOH indicators is closer to the exponential trend.

Disturbance of State of Charge to State of Health Indicators

Similarly, based on the experimental data of Cell 4, the evolution of SOH indicators at different SOC is also studied. As **Figures 7A,B** reveal, the disturbances of different SOC to the SOH indicators are roughly the same at each temperature within the operational temperature range of the battery (5–35°C). Thus, the experimental data at 25°C can be used for analysis, and the results can be applied to other temperatures. **Figures 7C and D** present the variations of the SOH indicators at different SOC at 25°C. Based on the variation

trends, the impacts of SOC on SOH indicators are both fitted with an exponential or quadratic relationship. Their expressions are illustrated as **Eqs. 26, 27**, respectively.

$$SOH = -0.1R_0 \times e^{-\mu SOC} + 0.4641C_d \times e^{-\sigma SOC} + 0.6255 + \delta, \quad (26)$$

$$SOH = -0.1R_0 \times (aSOC^2 + bSOC) + 0.4641C_d \times (cSOC^2 + dSOC) + \phi, \quad (27)$$

where $\mu, \sigma, \delta, a, b, c, d,$ and ϕ are the model parameters, and the fitting results are described as follows:

$$SOH = -0.1R_0 \times e^{0.2411SOC} + 0.4641C_d \times e^{-47.78SOC} + 1.0837. \quad (28)$$

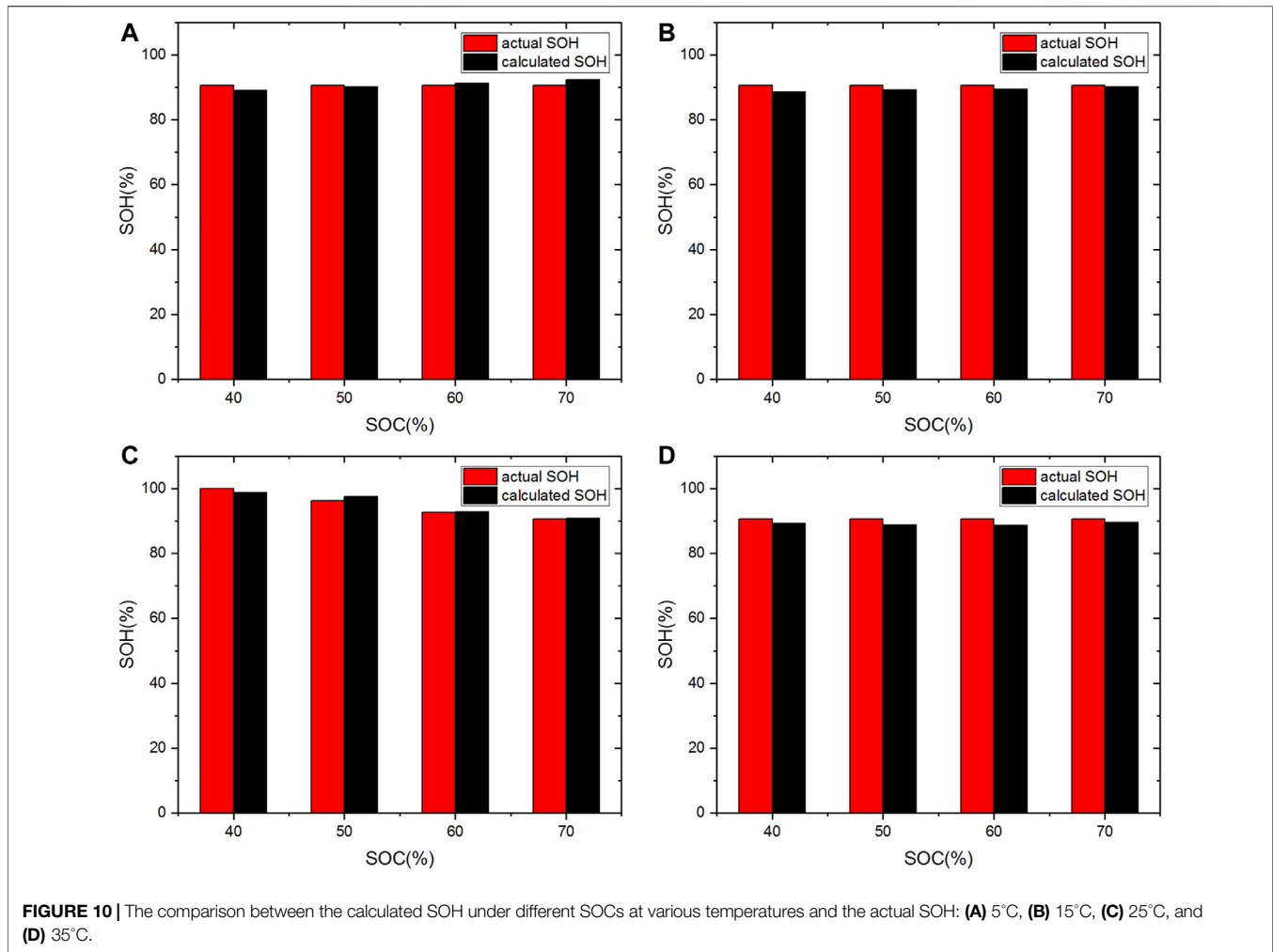
$$SOH = -0.1R_0 \times (-6.7SOC^2 + 7.2SOC) + 0.46C_d \times (-1.6SOC^2 + 1.6SOC) + 1.01. \quad (29)$$

The results of performing exponential and quadratic SOC factors are shown in **Figures 8C and D**, respectively. The comparison of errors is shown in **Figure 9B**, which reveals that the quadratic relationship between SOC and SOH indicators is in better agreement with the experimental data.

Final Definition of State of Health

Based on the above analysis, both temperature and the two SOH indicators are proven to be exponentially correlated, while both the SOC and the two SOH indicators are quadratically correlated. Finally, the definition of SOH considering the disturbance of temperature and SOC is established as **Eq. 30**.

$$SOH = -0.1R_0 \times (-4.8521SOC^2 + 5.5319SOC) e^{-1368.9\left(\frac{1}{T} - \frac{1}{T_{ref}}\right)} + 0.4641C_d \times (-1.2262SOC^2 + 1.2506SOC) e^{4280.9\left(\frac{1}{T} - \frac{1}{T_{ref}}\right)} + 0.9945. \quad (30)$$



The comparisons between the actual SOH and the estimated SOH at different SOC (40, 50, 60, and 70%) and temperatures (5, 15, 25, and 35°C) are shown in **Figure 10**. Among them, the actual SOH at 5, 15, and 35°C is 90.648%, and the maximum error is 2.301% under a specific operational condition (40% SOC, 15°C). Differently, the actual SOH at different SOC varies at 25°C to verify the applicability of the final SOH definition in different life stages. The actual SOH at SOC of 40, 50, 60, and 70% is 100, 96.29, 92.66, and 90.648%, respectively. In **Figure 10C**, it can be observed that the SOH calculated by **Eq. 30** is quite close to the actual SOH, and the maximum error is 1.276% at 40% SOC. This result indicates that the proposed indicators can be used for accurate SOH estimation considering different ambient temperatures and SOC.

CONCLUSION

In most cases, SOH estimation is conducted based on the battery capacity. However, the capacity estimation is difficult to be implemented online in EVs. Measurable SOH indicators from

ECM based on statistical analysis are proposed in this study. The main conclusions of this research are drawn as below:

- (1) The RLSM is utilized to identify the ECM parameters in UDDS and NEDC conditions. The identified values of R_0 , R_d , R_p , C_d , and C_p are verified with the fitting of the battery response voltage. The identification errors are within the tolerance.
- (2) With the battery aging, R_0 , R_p , and R_d increase, while C_p and C_d decrease. However, there are complicated coupling relationships between these ECM parameters. These coupling relationships are analyzed by MSRA and PA. According to the analysis results, R_0 and C_d are finally determined as SOH indicators. This conclusion applies to NCA batteries and LFP batteries with different nominal capacities.
- (3) R_0 and C_d fluctuate at ambient temperature and SOC. It is proved that the two SOH indicators and ambient temperature are both exponentially correlated, while the impacts of battery SOC on both R_0 and C_d present a quadratic trend. Accordingly, the final SOH definition considering the disturbance of temperature and SOC is established. The maximum error is 2.301% at 40% SOC and 15°C.

DATA AVAILABILITY STATEMENT

The raw data supporting the conclusions of this article will be made available by the authors, without undue reservation.

AUTHOR CONTRIBUTIONS

Conceptualization, GS, XW, and HD; Methodology, GS, SC, HY, HZY, XW, and HD; Investigation, GS, and HY; Writing–Original Draft, GS, XW, and HD; Writing–Review and Editing, GS, XW, SC, HY, HZY, XW, and HD; Supervision, XW and HD.

REFERENCES

- Agubra, V., and Fergus, J. (2013). Lithium Ion Battery Anode Aging Mechanisms. *Materials* 6 (4), 1310–1325. doi:10.3390/ma6041310
- Alwin, D. F., and Hauser, R. M. (1975). The Decomposition of Effects in Path Analysis. *Am. Sociological Rev.* 40 (1), 37–47. doi:10.2307/2094445
- Basia, A., Simeu-Abazi, Z., Gascard, E., and Zwolinski, P. (2021). Review on State of Health Estimation Methodologies for Lithium-Ion Batteries in the Context of Circular Economy. *CIRP J. Manufacturing Sci. Tech.* 32, 517–528. doi:10.1016/j.cirpj.2021.02.004
- Berecibar, M., Gandiaga, I., Villarreal, I., Omar, N., Van Mierlo, J., and Van den Bossche, P. (2016). Critical Review of State of Health Estimation Methods of Li-Ion Batteries for Real Applications. *Renew. Sust. Energ. Rev.* 56, 572–587. doi:10.1016/j.rser.2015.11.042
- Bloom, I., Jansen, A. N., Abraham, D. P., Knuth, J., Jones, S. A., Battaglia, V. S., et al. (2005). Differential Voltage Analyses of High-Power, Lithium-Ion Cells. *J. Power Sourc.* 139 (1), 295–303. doi:10.1016/j.jpowsour.2004.07.021
- Broussely, M., Biensan, P., Bonhomme, F., Blanchard, P., Herreyre, S., Nechev, K., et al. (2005). Main Aging Mechanisms in Li Ion Batteries. *J. Power Sourc.* 146 (1), 90–96. doi:10.1016/j.jpowsour.2005.03.172
- Chang, M.-T., Lin, Y.-S., Ling, S.-H., Liang, S.-H., Lin, C.-H., and Chen, K.-C. (2014). Identification of the Parameters in Equivalent Circuit Model of Lithium-Ion Batteries. *ECS Trans.* 61 (27), 125–130. doi:10.1149/06127.0125ecst
- Chen, S., Peng, X., Bao, N., and Garg, A. (2019). A Comprehensive Analysis and Optimization Process for an Integrated Liquid Cooling Plate for a Prismatic Lithium-Ion Battery Module. *Appl. Therm. Eng.* 156, 324–339. doi:10.1016/j.applthermaleng.2019.04.089
- Chen, Z., Mi, C. C., Fu, Y., Xu, J., and Gong, X. (2013). Online Battery State of Health Estimation Based on Genetic Algorithm for Electric and Hybrid Vehicle Applications. *J. Power Sourc.* 240, 184–192. doi:10.1016/j.jpowsour.2013.03.158
- Dai, H., Xu, T., Zhu, L., Wei, X., and Sun, Z. (2016). Adaptive Model Parameter Identification for Large Capacity Li-Ion Batteries on Separated Time Scales. *Appl. Energ.* 184, 119–131. doi:10.1016/j.apenergy.2016.10.020
- Deng, Z., Yang, L., Cai, Y., Deng, H., and Sun, L. (2016). Online Available Capacity Prediction and State of Charge Estimation Based on Advanced Data-Driven Algorithms for Lithium Iron Phosphate Battery. *Energy* 112, 469–480. doi:10.1016/j.energy.2016.06.130
- Galeotti, M., Cinà, L., Giammanco, C., Cordiner, S., and Di Carlo, A. (2015). Performance Analysis and SOH (State of Health) Evaluation of Lithium Polymer Batteries through Electrochemical Impedance Spectroscopy. *Energy* 89, 678–686. doi:10.1016/j.energy.2015.05.148
- Gomez, J., Nelson, R., Kalu, E. E., Weatherspoon, M. H., and Zheng, J. P. (2011). Equivalent Circuit Model Parameters of a High-Power Li-Ion Battery: Thermal and State of Charge Effects. *J. Power Sourc.* 196 (10), 4826–4831. doi:10.1016/j.jpowsour.2010.12.107
- Gu, W., Sun, Z., Wei, X., and Dai, H. (2014a). A Capacity Fading Model of Lithium-Ion Battery Cycle Life Based on the Kinetics of Side Reactions for Electric Vehicle Applications. *Electrochimica Acta* 133, 107–116. doi:10.1016/j.electacta.2014.03.186
- Gu, W., Sun, Z., Wei, X., and Dai, H. (2014b). A New Method of Accelerated Life Testing Based on the Grey System Theory for a Model-Based Lithium-Ion Battery Life Evaluation System. *J. Power Sourc.* 267, 366–379. doi:10.1016/j.jpowsour.2014.05.103
- Han, X., Ouyang, M., Lu, L., Li, J., Zheng, Y., and Li, Z. (2014). A Comparative Study of Commercial Lithium Ion Battery Cycle Life in Electrical Vehicle: Aging Mechanism Identification. *J. Power Sourc.* 251, 38–54. doi:10.1016/j.jpowsour.2013.11.029
- Hua, Y., Cordoba-Arenas, A., Warner, N., and Rizzoni, G. (2015). A Multi Time-Scale State-Of-Charge and State-Of-Health Estimation Framework Using Nonlinear Predictive Filter for Lithium-Ion Battery Pack with Passive Balance Control. *J. Power Sourc.* 280, 293–312. doi:10.1016/j.jpowsour.2015.01.112
- Jiang, B., Dai, H., Wei, X., and Xu, T. (2019). Joint Estimation of Lithium-Ion Battery State of Charge and Capacity within an Adaptive Variable Multi-Timescale Framework Considering Current Measurement Offset. *Appl. Energ.* 253, 113619. doi:10.1016/j.apenergy.2019.113619
- Kim, I. L.-S. (2010). A Technique for Estimating the State of Health of Lithium Batteries through a Dual-Sliding-Mode Observer. *IEEE Trans. Power Elect.* 25 (4), 1013–1022. doi:10.1109/TPEL.2009.2034966
- Li, W., Sengupta, N., Dechent, P., Howey, D., Annaswamy, A., and Sauer, D. U. (2021). Online Capacity Estimation of Lithium-Ion Batteries with Deep Long Short-Term Memory Networks. *J. Power Sourc.* 482, 228863. doi:10.1016/j.jpowsour.2020.228863
- Li, Z., Lu, L., Ouyang, M., and Xiao, Y. (2011). Modeling the Capacity Degradation of LiFePO₄/graphite Batteries Based on Stress Coupling Analysis. *J. Power Sourc.* 196 (22), 9757–9766. doi:10.1016/j.jpowsour.2011.07.080
- Liu, J., and Chen, Z. (2019). Remaining Useful Life Prediction of Lithium-Ion Batteries Based on Health Indicator and Gaussian Process Regression Model. *Ieee Access* 7, 39474–39484. doi:10.1109/access.2019.2905740
- Liu, K., Ashwin, T. R., Hu, X., Lucu, M., and Widanage, W. D. (2020a). An Evaluation Study of Different Modelling Techniques for Calendar Ageing Prediction of Lithium-Ion Batteries. *Renew. Sust. Energ. Rev.* 131, 110017. doi:10.1016/j.rser.2020.110017
- Liu, K., Hu, X., Wei, Z., Li, Y., and Jiang, Y. (2019). Modified Gaussian Process Regression Models for Cyclic Capacity Prediction of Lithium-Ion Batteries. *IEEE Trans. Transp. Electrific.* 5 (4), 1225–1236. doi:10.1109/TTE.2019.2944802
- Liu, K., Li, Y., Hu, X., Lucu, M., and Widanage, W. D. (2020b). Gaussian Process Regression with Automatic Relevance Determination Kernel for Calendar Ageing Prediction of Lithium-Ion Batteries. *IEEE Trans. Ind. Inf.* 16 (6), 3767–3777. doi:10.1109/TII.2019.2941747
- Nghiep, N., and Al, C. (2001). Predicting Housing Value: A Comparison of Multiple Regression Analysis and Artificial Neural Networks. *J. real estate Res.* 22 (3), 313–336. doi:10.1080/10835547.2001.12091068
- Pan, H., Lü, Z., Wang, H., Wei, H., and Chen, L. (2018). Novel Battery State-Of-Health Online Estimation Method Using Multiple Health Indicators and an Extreme Learning Machine. *Energy* 160, 466–477. doi:10.1016/j.energy.2018.06.220
- Park, E. S., Fitzpatrick, K., Das, S., and Avelar, R. (2021). Exploration of the Relationship Among Roadway Characteristics, Operating Speed, and Crashes

FUNDING

This work is financially supported by the National Natural Science Foundation of China (NSFC, grant nos. U20A20310 and U1764256)

SUPPLEMENTARY MATERIAL

The Supplementary Material for this article can be found online at: <https://www.frontiersin.org/articles/10.3389/fenrg.2021.690266/full#supplementary-material>

- for City Streets Using Path Analysis. *Accid. Anal. Prev.* 150, 105896. doi:10.1016/j.aap.2020.105896
- Park, K., Choi, Y., Choi, W. J., Ryu, H.-Y., and Kim, H. (2020). LSTM-based Battery Remaining Useful Life Prediction with Multi-Channel Charging Profiles. *Ieee Access* 8, 20786–20798. doi:10.1109/access.2020.2968939
- Ramadass, P., Haran, B., Gomadam, P. M., White, R., and Popov, B. N. (2004). Development of First Principles Capacity Fade Model for Li-Ion Cells. *J. Electrochem. Soc.* 151 (2), A196–A203. doi:10.1149/1.1634273
- Remmlinger, J., Buchholz, M., Meiler, M., Bernreuter, P., and Dietmayer, K. (2011). State-of-health Monitoring of Lithium-Ion Batteries in Electric Vehicles by On-Board Internal Resistance Estimation. *J. Power Sourc.* 196 (12), 5357–5363. doi:10.1016/j.jpowsour.2010.08.035
- Schmidt, C. L., and Skarstad, P. M. (1997). Development of an Equivalent-Circuit Model for the Lithium/iodine Battery. *J. Power Sourc.* 65 (1), 121–128. doi:10.1016/s0378-7753(96)02604-3
- Stage, F. K., Carter, H. C., and Nora, A. (2004). Path Analysis: An Introduction and Analysis of a Decade of Research. *J. Educ. Res.* 98 (1), 5–13. doi:10.3200/JOER.98.1.5-13
- Stolzenberg, R. M. (2004). “Multiple Regression Analysis,” in *Handbook of Data Analysis*. Editors M. Hardy and A. Bryman (Thousand Oaks, CA: Sage Publications), 165–208.
- Stroe, D. I., Swierczynski, M., Stan, A. I., Knap, V., Teodorescu, R., and Andreasen, S. J. (2014). “Diagnosis of Lithium-Ion Batteries State-Of-Health Based on Electrochemical Impedance Spectroscopy Technique,” in IEEE Energy Conversion Congress and Exposition (ECCE), Pittsburgh, PA, 4576–4582.
- Sun, F., and Xiong, R. (2015). A Novel Dual-Scale Cell State-Of-Charge Estimation Approach for Series-Connected Battery Pack Used in Electric Vehicles. *J. Power Sourc.* 274, 582–594. doi:10.1016/j.jpowsour.2014.10.119
- Takei, K., Seki, S., Mita, Y., Miyashiro, H., and Terada, N. (2011). “Investigations of Accelerated Life Evaluation Tests for High-Power Lithium-Ion Secondary Batteries for Plug-In Hybrid Electric Vehicles,” in Meeting Abstracts: The Electrochemical Society, Boston, MA, 1421.
- Tang, X., Wang, Y., Zou, C., Yao, K., Xia, Y., and Gao, F. (2019). A Novel Framework for Lithium-Ion Battery Modeling Considering Uncertainties of Temperature and Aging. *Energ. Convers. Manag.* 180, 162–170. doi:10.1016/j.enconman.2018.10.082
- Thomas, E. V., Bloom, I., Christophersen, J. P., and Battaglia, V. S. (2008). Statistical Methodology for Predicting the Life of Lithium-Ion Cells via Accelerated Degradation Testing. *J. Power Sourc.* 184 (1), 312–317. doi:10.1016/j.jpowsour.2008.06.017
- Wang, J., Liu, P., Hicks-Garner, J., Sherman, E., Soukiazian, S., Verbrugge, M., et al. (2011). Cycle-life Model for Graphite-LiFePO₄ Cells. *J. Power Sourc.* 196 (8), 3942–3948. doi:10.1016/j.jpowsour.2010.11.134
- Wang, T., Pei, L., Wang, T., Lu, R., and Zhu, C. (2015). On-Board State-Of-Health Estimation at a Wide Ambient Temperature Range in Lithium-Ion Batteries. *Energies* 8 (8), 8467–8481. doi:10.3390/en8088467
- Wang, X., Wei, X., and Dai, H. (2019). Estimation of State of Health of Lithium-Ion Batteries Based on Charge Transfer Resistance Considering Different Temperature and State of Charge. *J. Energ. Storage* 21, 618–631. doi:10.1016/j.est.2018.11.020
- Wang, X., Wei, X., Zhu, J., Dai, H., Zheng, Y., Xu, X., et al. (2021). A Review of Modeling, Acquisition, and Application of Lithium-Ion Battery Impedance for Onboard Battery Management. *eTransportation* 7, 100093. doi:10.1016/j.etrans.2020.100093
- Yun, Z., and Qin, W. (2020). Remaining Useful Life Estimation of Lithium-Ion Batteries Based on Optimal Time Series Health Indicator. *Ieee Access* 8, 55447–55461. doi:10.1109/access.2020.2981947
- Zenati, A., Desprez, P., Razik, H., and Rael, S. (2012). “A Methodology to Assess the State of Health of Lithium-Ion Batteries Based on the Battery’s Parameters and a Fuzzy Logic System,” in IEEE International Electric Vehicle Conference, Greenville, SC, 1–6.
- Zheng, X., and Fang, H. (2015). An Integrated Unscented Kalman Filter and Relevance Vector Regression Approach for Lithium-Ion Battery Remaining Useful Life and Short-Term Capacity Prediction. *Reliability Eng. Syst. Saf.* 144, 74–82. doi:10.1016/j.res.2015.07.013
- Zhou, Y., Huang, M., Chen, Y., and Tao, Y. (2016). A Novel Health Indicator for On-Line Lithium-Ion Batteries Remaining Useful Life Prediction. *J. Power Sourc.* 321, 1–10. doi:10.1016/j.jpowsour.2016.04.119

Conflict of Interest: The authors declare that the research was conducted in the absence of any commercial or financial relationships that could be construed as a potential conflict of interest.

Copyright © 2021 Shi, Chen, Yuan, You, Wang, Dai and Wei. This is an open-access article distributed under the terms of the Creative Commons Attribution License (CC BY). The use, distribution or reproduction in other forums is permitted, provided the original author(s) and the copyright owner(s) are credited and that the original publication in this journal is cited, in accordance with accepted academic practice. No use, distribution or reproduction is permitted which does not comply with these terms.

GLOSSARY

SOH State of health

SOC State of charge

EVs Electric vehicles

ECM Equivalent circuit model

LFP Lithium iron phosphate

NCA Nickel–cobalt–aluminum

RPT Reference performance test

NEDC New European Driving Cycle

UDDS Urban Dynamometer Driving Schedule

OCV Open circuit voltage

RLSM Recursive least square method

PCA Principal component analysis

CA Correlation analysis

MSRA Multiple stepwise regression analysis

PA Path analysis

BMS Battery management system

R_0 Ohmic resistance (Ω)

R_p Polarization resistance (Ω)

R_d Diffusion resistance (Ω)

C_p Polarization capacitance (F)

C_d Diffusion capacitance (F)

E_0 OCV of the cell (V)

I Load current (A)

U Terminal voltage (V)

E_t Response voltage (V)

t_s The sampling time (s)

x_i Independent variable

y Dependent variable

σ_{x_i} Standard deviation

$b_i \frac{\sigma_{x_i}}{\sigma_y}$ Standardized partial regression coefficient

r_{ij} Correlation coefficient between variables x_i and x_j

P_{iY} Direct path coefficient

$r_{ij}P_{jY}$ Indirect path coefficient

T Absolute temperature (K)

T_{ref} Reference temperature (298.15K).